

Submillimetre observations of galaxy clusters with the BLAST: the star formation activity in Abell 3112

Filiberto G. Braglia,^{1*} Peter A. R. Ade,² James J. Bock,³ Edward L. Chapin,¹ Mark J. Devlin,⁴ Alastair Edge,⁵ Matthew Griffin,² Joshua O. Gundersen,⁶ Mark Halpern,¹ Peter C. Hargrave,² David H. Hughes,⁷ Jeff Klein,⁴ Gaelen Marsden,¹ Philip Maukopf,² Lorenzo Moncelsi,² Calvin B. Netterfield,^{8,9} Henry Ngo,¹ Luca Olmi,^{10,11} Enzo Pascale,² Guillaume Patanchon,¹² Kevin A. Pimblet,^{13†} Marie Rex,¹⁴ Douglas Scott,¹ Christopher Semisch,⁴ Nicholas Thomas,⁶ Matthew D. P. Truch,⁴ Carole Tucker,² Gregory S. Tucker,¹⁵ Elisabetta Valiante,¹ Marco P. Viero¹⁶ and Donald V. Wiebe¹

¹Department of Physics & Astronomy, University of British Columbia, 6224 Agricultural Road, Vancouver, BC V6T 1Z1, Canada

²School of Physics & Astronomy, Cardiff University, 5 The Parade, Cardiff CF24 3AA

³Jet Propulsion Laboratory, Pasadena, CA 91109-8099, USA

⁴Department of Physics & Astronomy, University of Pennsylvania, 209 South 33rd Street, Philadelphia, PA 19104, USA

⁵Department of Physics, Durham University, South Road, Durham DH1 3LE

⁶Department of Physics, University of Miami, 1320 Campo Sano Drive, Coral Gables, FL 33146, USA

⁷Instituto Nacional de Astrofísica Óptica y Electrónica (INAOE), Aptdo. Postal 51 y 72000 Puebla, Mexico

⁸Department of Astronomy & Astrophysics, University of Toronto, 50 St George Street Toronto, ON M5S 3H4, Canada

⁹Department of Physics, University of Toronto, 60 St George Street, Toronto, ON M5S 1A7, Canada

¹⁰Physics Department, University of Puerto Rico, Río Piedras Campus, Box 23343, UPR station, PR 00931, USA

¹¹INAF - Osservatorio Astrofisico di Arcetri, Largo E. Fermi 5, I-50125 Firenze, Italy

¹²Université Paris Diderot, Laboratoire APC, 10, rue Alice Domon et Léonie Duquet, 75205 Paris, France

¹³School of Physics, Monash University, Clayton, VIC 3800, Australia

¹⁴Steward Observatory, University of Arizona, 933 N. Chery Ave, Tucson, AZ 85721, USA

¹⁵Department of Physics, Brown University, 182 Hope Street, Providence, RI 02912, USA

¹⁶California Institute of Technology, 1200 E. California Blvd, Pasadena, CA 91125, USA

Accepted 2010 November 3. Received 2010 November 2; in original form 2010 March 9

ABSTRACT

We present observations at 250, 350 and 500 μm of the nearby galaxy cluster Abell 3112 ($z = 0.075$) carried out with the Balloon-borne Large Aperture Submillimeter Telescope. Five cluster members are individually detected as bright submillimetre (submm) sources. Their far-infrared spectral energy distributions and optical colours identify them as normal star-forming galaxies of high mass, with globally evolved stellar populations. They all have ($B - R$) colours of 1.38 ± 0.08 , transitional between the blue, active population and the red, evolved galaxies that dominate the cluster core. We stack to estimate the mean submm emission from all cluster members, which is determined to be 16.6 ± 2.5 , 6.1 ± 1.9 and 1.5 ± 1.3 mJy at 250, 350 and 500 μm , respectively. Stacking analyses of the submm emission of cluster members reveal trends in the mean far-infrared luminosity with respect to clustercentric radius and K_S -band magnitude. We find that a large fraction of submm emission comes from the boundary of the inner, virialized region of the cluster, at clustercentric distances around R_{500} . Stacking also shows that the bulk of the submm emission arises in intermediate-mass galaxies with K_S magnitude ~ 1 mag fainter than the characteristic magnitude K_S^* . The results and

*E-mail: fbraglia@phas.ubc.ca

†Correction added after online publication 2011 February 22: author affiliation amended.

constraints obtained in this work will provide a useful reference for the forthcoming surveys to be conducted on galaxy clusters by *Herschel*.

Key words: galaxies: clusters: general – galaxies: clusters: individual: A3112 – galaxies: evolution – galaxies: star formation – infrared: galaxies – submillimetre: galaxies.

1 INTRODUCTION

The evolution of cluster galaxies and their star formation rates (SFRs) have been studied using several different approaches in the last few decades. Optical surveys have shown clear correlations between galaxy colours and the local galaxy density or clustercentric radius (Dressler 1980; Dressler et al. 1997; Kodama et al. 2001). Spectroscopic observations have consistently identified trends in the star formation activity of cluster galaxies, both as a function of the clustercentric distance (e.g. Verdugo, Ziegler & Gerken 2008; Braglia et al. 2009 and references therein) and at different redshifts (Poggianti et al. 2006, 2009). Variation in the SFR and correlation with the local environment has also been investigated at different mass scales, from groups (Wilman et al. 2008) to large superclusters (Porter & Raychaudhury 2007), and also in relation to local large-scale filamentary structures (Braglia, Pierini & Böhringer 2007; Porter et al. 2008).

Observations with the *IRAS* and *ISO* provided a way to investigate the nature of dust and to correlate the SFRs of cluster galaxies with their dust content, albeit mostly covering the spectral regions dominated by warm (>40 K) dust (see Metcalfe, Fadda & Biviano 2005 for a review of the results on galaxy clusters obtained with the *ISO*). While part of these studies was aimed at detecting diffuse emission from warm intracluster dust (e.g. Stickel et al. 1998, 2002; Montier & Giard 2005; Giard et al. 2008), several results were also obtained with observations of individual cluster members in several clusters. Edge (2001) used combined *IRAS*, IRAM and JCMT observations to detect CO line emission from molecular gas in the central galaxies of a sample of 16 cooling core galaxies. Tuffs et al. (2002) and Popescu et al. (2002a,b) observed a large sample of galaxies in Virgo, finding a dependence of the dust content of galaxies with Hubble type. Pierini & Möller (2003) found that dust luminosity and mass depend on galaxy geometry and shape as well as stellar mass.

Several recent 24- μm observations with *Spitzer*-MIPS have detected dusty star-forming galaxies in intermediate- to high- z clusters. Geach et al. (2006) find an increase in the total SFR in clusters with increasing redshift from *Spitzer* observations, although with large scatter. Bai, Rieke & Rieke (2007) investigate the infrared (IR) properties and the mid-IR luminosity function in a higher redshift cluster at $z = 0.83$, confirming the presence of evolution in the SFR of cluster galaxies. Fadda et al. (2008) identify consistent overdensities of 24- μm sources along two filaments between the clusters Abell 1770 and Abell 1763 ($z = 0.23$) with respect to the surrounding field. Similar to Bai et al. (2007), Haines et al. (2009a) confirm an excess of 24- μm sources in the cluster Abell 1758 at $z = 0.28$. Tran et al. (2009) also compare the 24- μm luminous members of a cluster, a supergroup and the field, concluding that the mid-IR inferred SFR is higher in the intermediate environment of the groups than in the field, while it is globally lower in the cluster. Local dependence of the density of 24- μm sources in clusters is investigated in the LoCuSS survey by Haines et al. (2009b) who find a global decrease in star-forming systems with decreasing clustercentric radius.

Recently, Wardlow et al. (2010) have used the AzTEC camera to observe a field centred on the cluster MS0451.6–0305 at $z = 0.54$, identifying two luminous IR galaxies (LIRGs) with a combined SFR of around $100 M_{\odot} \text{ yr}^{-1}$. They suggest that, if these are indeed cluster members, they can be examples of a population of galaxies undergoing transformation to the red sequence (RS) through interaction with the cluster environment.

The largest part of these previous studies conducted on clusters have investigated the star formation activity of cluster galaxies either in the mid-IR or at millimetre wavelengths. However, a complete characterization of the output of star formation requires coverage of the rest-frame $\sim 100 \mu\text{m}$ spectral region, where the peak of the far-IR emission is expected to lie.

The Balloon-borne Large Aperture Submillimeter Telescope (BLAST: Pascale et al. 2008; Devlin et al. 2009) is a pathfinder experiment to *Herschel*/SPIRE and has provided the first maps of selected areas of the sky at 250, 350 and 500 μm . These wavelengths were mainly chosen to constrain the peak of the far-IR emission from galaxies at redshifts $z \gtrsim 1$. Several studies carried out by the BLAST collaboration on extragalactic fields, either on individual sources (Dunlop et al. 2010; Dye et al. 2009; Ivison et al. 2010), using stacking (Devlin et al. 2009; Marsden et al. 2009; Pascale et al. 2009; Ivison et al. 2010), or on other statistical analyses (Patanchon et al. 2009; Viero et al. 2009), have been performed on blank-field maps. A few other studies (Rex et al. 2009; Wiebe et al. 2009) have been conducted on known targets. In particular, Rex et al. have provided the first submillimetre (submm) maps of the ‘Bullet’ cluster (Tucker et al. 1998), investigating the nature of a bright submm source identified as a counterpart of a lensed high- z star-forming galaxy.

We present here 250-, 350- and 500- μm observations of a field centred on the nearby cluster Abell 3112 ($z = 0.075$; hereinafter A3112) carried out by the BLAST and the results of a combined analysis of the optical and submm properties of a spectroscopic sample of its cluster members. These results demonstrate that observations of cluster galaxies at submm wavelengths can provide insight into the star formation activity in clusters and help in understanding galaxy evolution within these overdense environments.

This paper is organized as follows. Section 2 introduces the BLAST observations of A3112, and the ancillary optical and near-IR data used for our study. Section 3 shows the results from stacking analyses of cluster member catalogues and the properties of submm bright cluster members. These results are discussed in Section 4 and summarized in Section 5.

Throughout this paper, we use a standard Λ cold dark matter cosmology, where $\Omega_M = 0.3$, $\Omega_{\Lambda} = 0.7$ and $h \equiv H_0/100 \text{ km s}^{-1} \text{ Mpc}^{-1} = 0.7$.

2 OBSERVATIONS AND DATA

2.1 BLAST

The BLAST stratospheric telescope has a 1.8-m primary mirror and three broad-band bolometer arrays that observe the sky

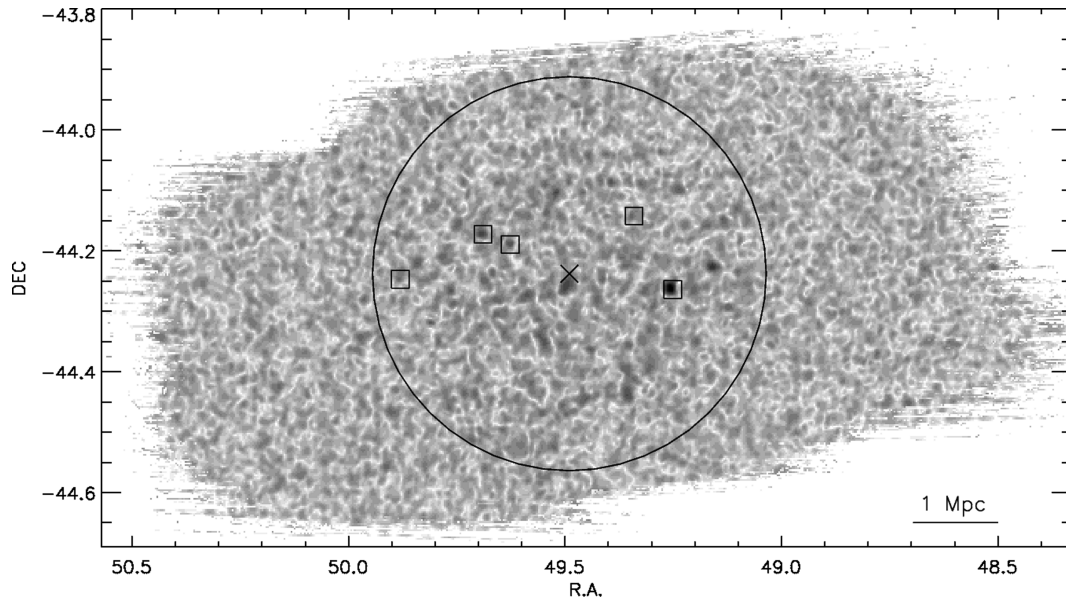


Figure 1. BLAST total S/N map of A3112. The circle marks $R_{200} = 1.79$ Mpc (as calculated from cluster members dynamics, cf. Section 3.1). The boxes mark the position of BLAST sources identified as cluster members (Section 3.2). The cross marks the position of the brightest cluster galaxy and the cluster centre. The distance scale is calculated at the cluster redshift of 0.075.

simultaneously at 250, 350 and 500 μm . This array system is effectively a prototype of the SPIRE instrument onboard the *Herschel* satellite. The instrument beams are nearly diffraction-limited and are approximately described as Gaussians with full width at half-maximum (FWHM) of 36, 42 and 60 arcsec at 250, 350 and 500 μm , respectively. For an extended description of the instrument, data analysis and calibration procedures, see Pascale et al. (2008) and Truch et al. (2009).

A large fraction of the successful BLAST observational campaign of 2006 (BLAST06) from the McMurdo Station, Antarctica, was dedicated to completing deep and wide blank-field extragalactic surveys. Smaller fields centred on the positions of well-known targets were also observed (e.g. Rex et al. 2009; Wiebe et al. 2009). Among those was a 1.1 – deg^2 field centred on the nearby cluster A3112 at $z = 0.075$, which was observed for a total time of 4.2 h. The original aim of these observations was the detection of submm emission from the central galaxy, for which a wide range of multiwavelength data are available, while at the same time being able to collect emission from potential cluster members out to R_{200} , as the low redshift implies that individual sources at the distance of the cluster can be detected at BLAST wavelengths (Fig. 1). The favourable declination also allowed a suitable observation window during the stratospheric flight from Antarctica and the high value of $|b|$ assured that the observed field is relatively clean of Galactic cirrus.

The BLAST time-stream data were reduced using a common pipeline to identify spikes, correct detector time drift and calibrate data (Pascale et al. 2008; Truch et al. 2009). Maps were generated using the SANEPIC software, which uses a maximum-likelihood algorithm to estimate the optimal solution for the map, as well as producing an associated noise map (Patanchon et al. 2008). Absolute calibration is based on observations of the evolved star VY CMa and is estimated to be at the level of 10 per cent (although strongly correlated between the three bands; see Truch et al. 2009 for details).

2.1.1 Maps

While the maps represent the optimal weighting of the data across all spatial scales, the largest scales are less constrained due to various systematic effects, particularly because of the lack of cross-linking in the scans of this particular field. This can produce residual large-scale fluctuating patterns across the map. To suppress these spurious signals, all maps have been filtered to remove low spatial frequencies without affecting the sources, corresponding to scales in excess of about 10 arcmin (approximately the size of the detector array projected on the sky). This procedure, already used for the BLAST GOODS-S (BGS) maps (e.g. Devlin et al. 2009), also explicitly sets the mean of each map to zero. We obtain 1σ noise values of 27.3, 21.3 and 15.6 mJy at 250, 350 and 500 μm , respectively, in the central 0.8 deg^2 of the observed field.¹ This is an area comparable to the BGS-Deep map. An outer, shallower region of about 0.3 deg^2 total area was also observed, albeit with higher noise: we calculate 1σ map rms values of 63.8, 58.6 and 39.0 mJy for this region. Due to the high noise of the wider area, we only include it in the stacking analyses where it can be appropriately weighted; source extraction is performed only in the deeper region to ensure robust identifications.

Analysis of the signal-to-noise ratio (S/N) maps shows that the observations of A3112 are not strongly dominated by confusion. The distribution of the S/N is well described by a Gaussian with a wing towards high positive values (due to bright sources in the maps), whose width only slightly exceeds pure instrumental noise. We evaluate the contribution of confusion to the total measured noise, measured as $\sigma_{\text{conf}}/\sigma_{\text{map}}$, as 24, 26 and 29 per cent at 250, 350 and 500 μm , respectively. Fig. 2 shows the distribution of the S/N at 250 μm .

¹ BLAST maps and point spread functions (PSFs) of A3112 are available for download at <http://blastexperiment.info>.

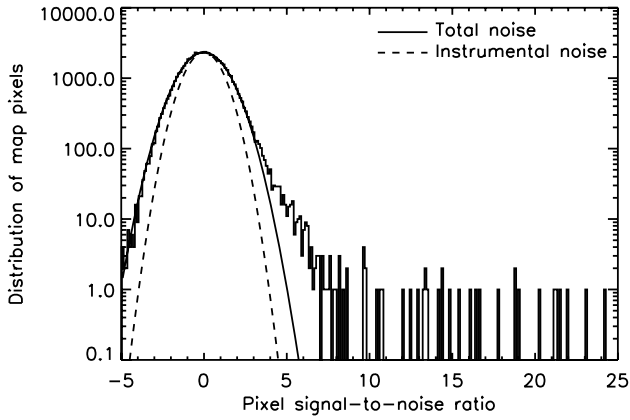


Figure 2. Distribution of the S/N in the 250- μm map of A3112. The solid line shows the Gaussian fit to the noise distribution, yielding the total map noise at 250 μm , while the dashed line shows the instrumental noise of the map, with width of 1 in units of S/N. Although the map shows a component of confusion noise, the instrumental noise dominates.

2.1.2 Source extraction

Individual BLAST sources are extracted from each map using a source-finding algorithm, which identifies peaks in a smoothed map produced by convolving the flux density map (weighted by the inverse of the variance) with the PSF of the BLAST. Peaks with an S/N of at least 3 are selected as sources and their flux is then calculated as the value of the beam-convolved flux density map at the position of the peak. The positional uncertainty is calculated as in Ivison et al. (2007), where we assume the slope of the number counts from Patanchon et al. (2009) and a minimum positional uncertainty of 5 arcsec is imposed, equal to the intrinsic pointing uncertainty of the instrument. The positional uncertainty lies below 8, 9 and 13 arcsec for 5σ (or more) sources at 250, 350 and 500 μm , respectively. Sources at different wavelengths are associated on the basis of their peak position, as in Devlin et al. (2009); the source catalogues are provided in Table 1.

We identify 86, 74 and 46 sources at 250, 350 and 500 μm , respectively, with S/N values in excess of 3 and up to 23. We use the results of Patanchon et al. (2009) to predict the number of sources expected for a blank field with the same area and depth as the A3112 observations. We find expected numbers of 37_{-14}^{+18} , 22_{-16}^{+30} and 20_{-17}^{+41} sources at 250, 350 and 500 μm , respectively. Despite the relatively large errors on the predicted number counts, the number

of sources detected at 250 μm exceeds the expected number by a factor of 2. The excess decreases at longer wavelengths to become completely consistent with the expected counts at 500 μm . This suggests that the excess detected is mainly due to the presence of the cluster, whose population should be detected preferentially at 250 μm .

2.1.3 Stacking

Robust association of optical counterparts to BLAST sources is usually possible only for very robust detections and relies on a number of assumptions and on the use of ancillary data (cf. Section 3.2). Moreover, the map noise will prevent the detection of individual faint sources. It is nevertheless possible to obtain robust statistical information about the average BLAST flux density of a sample of counterparts by *stacking* the BLAST maps on a provided catalogue. This technique has been described in great detail by Marsden et al. (2009) and was successfully used to determine the intensity of the far-IR background using BLAST data in the BGS field (Devlin et al. 2009; Marsden et al. 2009; Pascale et al. 2009). Stacking will be applied in Sections 3.1, 3.4 and 3.5.

2.2 Ancillary data

BLAST data were combined with optical spectroscopy to identify cluster members and ultraviolet-to-near-IR (UV-to-near-IR) photometry was used to characterize the cluster members on the basis of their photometric properties. This allows us to investigate the far-IR star formation activity of cluster galaxies together with their unobscured UV star formation and classification from multiband photometry.

We collected spectroscopic redshifts in the field of A3112 from dedicated observations of the AAOmega Spectrometer on the Anglo-Australian Telescope (AAT). AAOmega (Sharp et al. 2006) is the new fibre-fed spectrograph for the 2dF robot fibre positioner. It has 392 fibres covering a total area of 2 deg²; a dichroic allows continuous coverage of the spectral region from 3700 to 8800 Å with a resolution $\lambda/\delta\lambda = 1300$. Data were collected with service observations on 2009 November 24 (Proposal ID A103, PI: FGB) for a total of 5.1 h. Target selection was based on available photometry (see below) to select potential cluster members from optical and near-IR colours.

Two instrumental setups allowed us to collect 683 spectra. Data reduction was performed using the standard AAOmega pipeline,

Table 1. Combined BLAST catalogue of objects in the field of A3112. Flux densities and errors are given in Jy. Where flux densities are given in more than one band, the quoted position is the averaged position of the matched sources. An asterisk (*) following the BLAST ID means the source is identified as a counterpart of a cluster member (cf. Section 3.2.1). The full table is available as online Supporting Information.

	BLAST ID	RA	Dec.	S_{250}	δS_{250}	S_{350}	δS_{350}	S_{500}	δS_{500}
1	BLAST J031700–441605*	49.250954	–44.268158	0.665	0.029	0.245	0.022	0.079	0.016
2	BLAST J031844–441044*	49.686970	–44.179085	0.195	0.028	0.106	0.021	0.063	0.016
3	BLAST J031829–441138*	49.622036	–44.193897	0.181	0.028	0.090	0.021	0.054	0.015
4	BLAST J031746–442706	49.443359	–44.451836	0.188	0.030	–	–	–	–
5	BLAST J031733–440535	49.388805	–44.093178	0.173	0.028	0.072	0.022	–	–
6	BLAST J031803–440636	49.514664	–44.110165	0.167	0.028	0.096	0.022	–	–
7	BLAST J031754–441546	49.478020	–44.262951	0.159	0.027	–	–	–	–
8	BLAST J031930–441512*	49.877411	–44.253513	0.195	0.034	–	–	–	–
9	BLAST J031636–441359	49.153713	–44.233124	0.176	0.032	0.189	0.025	–	–
10	BLAST J031913–441933	49.804504	–44.325981	0.160	0.030	–	–	–	–

2dfdr, available on the AAOmega website.² Redshifts were extracted using standard IRAF tasks and then checked individually. We obtained redshifts for 578 out of 683 spectra (a success rate of 87 per cent), with 550 reliable non-stellar spectra.

Additional spectroscopic redshifts in the field were collected from the NASA/IPAC Extragalactic Data base (NED). Most of these are from the Las Campanas Redshift Survey (LCRS, Shectman et al. 1996) and from the Two-Degree Field survey (2dF, Colless et al. 2001). A total of 188 redshifts were obtained for this field, with a redshift range of 0–0.22, from which we identified 90 galaxies not covered by the AAOmega observations, for a total of 640 redshifts within 0.8 from the cluster centre.

Optical photometry in the Harris *B* and *R* passbands is available from dedicated observations of A3112 carried out at the Las Campanas Observatory Swope Telescope within the Las Campanas/AAT Rich Cluster Survey (LARCS; Pimbblet et al. 2001, 2002). These two filters cover the spectral region from 3500 to 6800 Å, which includes a number of important spectral features for galaxies at low redshift. In particular, the two filters bracket the 4000 Å break for galaxies at the redshift of A3112, thus providing a classification of galaxies with respect to their global, unobscured star formation activity by means of the *B* – *R* colour. Near-IR photometry was extracted from the Two-Micron All-Sky Survey (2MASS) data base (Skrutskie et al. 2006), providing *J*-, *H*- and *K_S*-band photometry for all cluster members. We used the magnitude values from the Extended Source Catalogue (XSC) where available; where the objects were not present in this catalogue, the Point Source Catalogue (PSC) was used instead. Undetected galaxies were assigned an upper magnitude limit consistent with the 2MASS limits. *GALEX* near- and far-UV photometry was obtained from the Nearby Galaxy Survey (NGS) in the GR4/5 data release. Where no significant UV flux was detected, we assigned an upper limit consistent with the NGS limits in the field of A3112. All optical and near-IR magnitudes were converted to the AB system.

3 RESULTS

3.1 Cluster members and specific SFR

Optical cluster members were identified using the weighted gap selection technique outlined by Girardi et al. (1993), after removing all objects with velocity differences larger than 4000 km s⁻¹ from the robust cluster redshift $z = 0.0756 \pm 0.0022$; the phase-space rejection criterion of Katgert, Biviano & Mazure (2004) was then applied to the survivors to reject less-evident interlopers (see also den Hartog & Katgert 1996). We identify 146 dynamically bound optical cluster members in the field observed with the BLAST, scattered across the cluster area from its core to a maximum distance of $3.4 h^{-1}$ Mpc (at the cluster redshift), with a robust velocity dispersion of 615 ± 34 km s⁻¹. We assumed the position of the central galaxy, which corresponds to the central peak of X-ray emission (within 8 kpc at the cluster redshift), as the cluster centre. Fig. 3 shows the distribution of confirmed cluster members in phase space.

Kinematic information from the confirmed cluster members was used to derive the cluster dynamical mass using the recipes summarized by Biviano et al. (2006). We derive a dynamical mass of $(4.2 \pm 0.5) \times 10^{14} M_{\odot}$ within $R_{200} = 1.79 h^{-1}$ Mpc (R_{200} is the radius where the overdensity of the cluster with respect to the cosmic

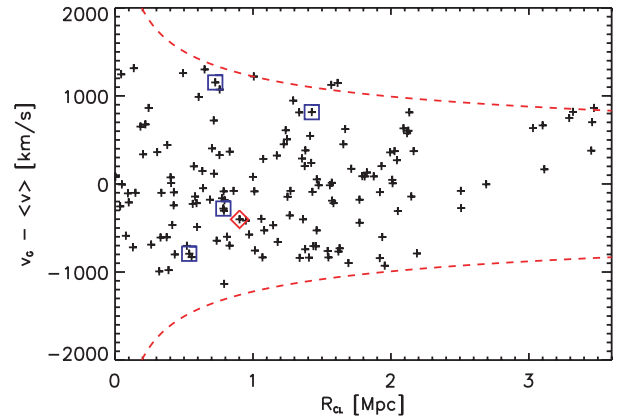


Figure 3. The distribution of confirmed cluster members in the velocity versus clustercentric distance plane. The squares mark the position of BLAST counterparts and the diamond marks the *IRAS* source IRAS 03152–4427 (cf. Section 3.2). The red dashed lines mark the cluster caustics as defined by Katgert et al. (2004).

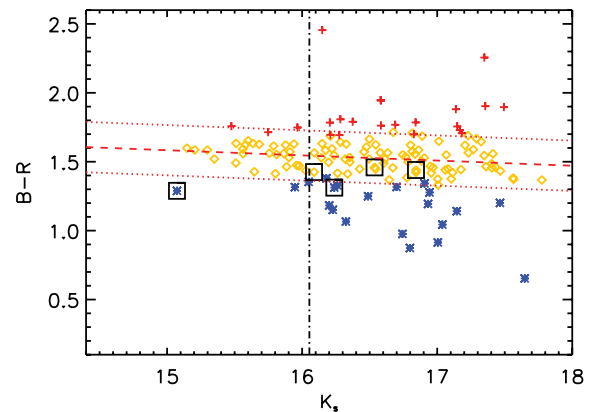


Figure 4. Cluster members in the (*B* – *R*) versus *K_S* plane. The dashed line shows the fit of the RS with $\pm 3 \sigma$ limits shown by dotted lines. Yellow diamonds mark the galaxies along the RS and blue stars the blue star-forming galaxies. Objects redder than the RS are shown as red crosses. The black boxes mark the positions of cluster members identified as BLAST counterparts (Sections 3.2 and 3.3). The vertical dot–dashed line marks the value of K_S^* , as defined in the text.

background density exceeds 200). This value and the cluster X-ray luminosity of 4.2×10^{37} W ($1.1 \times 10^{11} L_{\odot}$) (Böhringer et al. 2004) identify A3112 as an intermediate-mass system.

We fit the cluster RS in the (*B* – *R*) versus *K_S* plane. This allows for galaxy classification to be carried out independently with respect to stellar mass (traced by the *K_S* magnitude) and to the unobscured star formation activity (whose signature can be identified in the *B* – *R* colour), thus minimizing any residual colour term in the colour–magnitude plane. We fit the RS through a recursive 3σ -clipping algorithm, which converges to the fit

$$RS_{(B-R)} = 2.15 - 0.04 \times K_S. \quad (1)$$

Fig. 4 shows the cluster colour–magnitude diagram. We assume as a reference for K_S^* the value³ obtained by Cole et al. (2001) (converted to the AB system) for a large sample of galaxies from the 2MASS.

³ K_S^* is the characteristic Schechter magnitude, that is, the magnitude of the high-luminosity cut-off in the power-law profile of the Schechter luminosity function of the cluster, calculated in the *K_S* band.

² <http://www.aao.gov.au/AAO/2df/aaomega/aaomega.html>

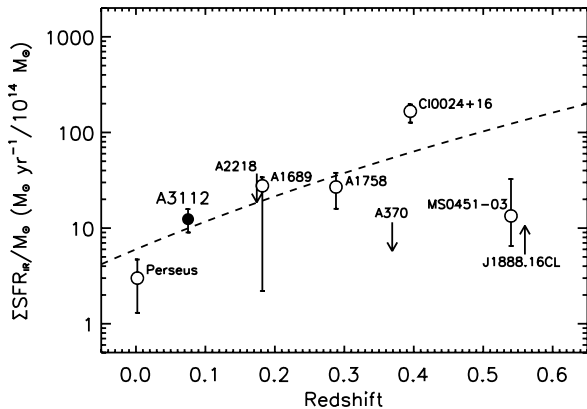


Figure 5. The position of A3112 (black circle) in the SSFR versus z plane. Open circles are data points from Geach et al. (2006) and Haines et al. (2009b); the dashed line shows the evolutionary model of Cowie et al. (2004). A3112 agrees closely with the relation found for the evolution of the SFR with redshift.

Out of the 146 identified cluster members, 99 lie along the RS, while 21 of them populate the colour–magnitude plane below the RS (see Fig. 4). Interestingly, a similar number of cluster members (26) lie above the RS. These very red galaxies could, in principle, be either young and dusty or very old evolved galaxies whose dust reservoir is completely depleted. BLAST observations are a powerful tool to solve this degeneracy without the need for optical spectroscopy, since submm emission is a direct probe of dust.

We derive the unobscured SFR of each cluster member from *GALEX* broad-band photometry, using the approach described by Schiminovich et al. (2005). On average, cluster galaxies have negligible or very small ($<1 M_{\odot} \text{ yr}^{-1}$) SFRs. However, 15 cluster members (i.e. about 9 per cent of our sample) show moderate SFRs ($\gtrsim 5 M_{\odot} \text{ yr}^{-1}$).

We also calculate the stellar mass of cluster members from K_S photometry using the same recipe as provided by Arnouts et al. (2007). We assume the relation for active/blue galaxies (parameter set 1 in Arnouts et al. 2007) for galaxies below the RS and the relation for quiescent/red galaxies (parameter set 2) for galaxies along and above the RS. We obtain stellar masses across two orders of magnitude from $7 \times 10^8 M_{\odot}$ for the smallest galaxies in our sample to $1.8 \times 10^{10} M_{\odot}$ for the central galaxy.

We stack the BLAST flux density maps on the cluster member catalogue to assess the mean flux density in the three BLAST bands. We obtain stacked values of 16.6 ± 2.5 , 6.1 ± 1.9 and 1.5 ± 1.3 mJy at 250, 350 and 500 μm , respectively. This converts to a mean SFR of $0.4 M_{\odot} \text{ yr}^{-1}$ per cluster member and a total SFR of $58 M_{\odot} \text{ yr}^{-1}$ for the whole sample of cluster members. We thus calculate a specific SFR (SSFR), $\Sigma\text{SFR} = \text{SFR}^{\text{tot}} / (M_{\text{dyn}} / 10^{14} M_{\odot}) = 12.4 \pm 3.4 \text{ yr}^{-1}$. This is in very good agreement with the relation found by Cowie et al. (2004) as shown in Fig. 5 (cf. Geach et al. 2006 and Haines et al. 2009b).

3.2 Individual sources

3.2.1 Star-forming galaxies in the cluster

Far-IR spectral energy distributions (SEDs) have been fitted to cluster members identified as BLAST counterparts to help identify their nature. The direct association of optical objects with submm sources is usually far from trivial, mainly due to the large beam size in the submm. Ideally, radio observations would be required to pinpoint

the precise position to be matched with optical catalogues (Dye et al. 2009; Ivison et al. 2010). However, we note that in the field of A3112, in each case that a robust ($\geq 5\sigma$) 250- μm source is detected, an optical cluster member is present within 1σ of the positional uncertainty from the source peak. Moreover, these BLAST sources are all found to be brighter at 250 μm than at 350 or 500 μm , suggesting that they originate from low-redshift galaxies. As shown later, these sources are found to have low temperatures ($T \lesssim 20$ K), consistent with being quiescent star formers at the cluster redshift. Moreover, for these sources, a single counterpart is usually detected within the positional uncertainty, ruling out the presence of other low- z galaxies not associated with the cluster that could contribute to the submm signal. We thus conclude that for the scope of this work, when these criteria are met (i.e. robust detection of a 250- μm BLAST source and presence of a single optical counterpart within the positional uncertainty), association of optical cluster members to BLAST sources can be considered robust. In addition to 5σ detections at 250 μm , we also include sources with a $>4\sigma$ detection both at 250 and 350 μm , to increase the number of confirmed counterparts while still maintaining a criterion of robustness. We thus select five galaxies shown in Fig. 6 and whose data appear in Table 2. Of these five galaxies, BLAST J031700–441605 is also an *IRAS* source, IRAS 03152–4427. Several other bright galaxies have good positional matches with BLAST sources; however, they are either not robustly detected (i.e. $<4\sigma$) at BLAST wavelengths or not cluster members or missing a spectroscopic redshift altogether. We do not include these galaxies in our analysis to avoid biasing our results.

SEDs are fitted using the same method as explained and used in Chapin et al. (2008), taking into account filter response curves, calibration uncertainties and correlations between the BLAST maps (Truch et al. 2009). Since we have only a modest range of far-IR/submm wavelengths (the three BLAST bands), we do not fit the dust emissivity index β (i.e. the slope of the modified blackbody); instead, we fix it to 2, according to the results of Wiebe et al. (2009). Far-IR luminosity and dust mass are derived from the SED, and we use the relation by Bell (2003) to derive the SFR from the far-IR luminosity. The results of the fit are shown in Fig. 7.

For IRAS 03152–4427, data at 60 and 100 μm are also available from the *IRAS* Faint Source Catalogue (Moshir et al. 1990). In particular, 100- μm data allow for better constraints on the shape of the far-IR SED (the 60- μm point already samples the warm dust emission and is not suitable to fit a single-component SED). We find for IRAS 03152–4427 a best-fitting temperature $T = (23.4 \pm 0.8)$ K, a total far-IR luminosity of $(1.2 \pm 0.1) \times 10^{11} L_{\odot}$, a cold dust mass of $(1.7 \pm 0.1) \times 10^8 M_{\odot}$ and an SFR of $(20.2 \pm 1.9) M_{\odot} \text{ yr}^{-1}$. This source is thus identified as a LIRG with moderate star formation. If the SFR derived from the UV ($19.4 \pm 0.2 M_{\odot} \text{ yr}^{-1}$, cf. Section 2.2) is added, then we obtain a total SFR of $(39.6 \pm 2.0) M_{\odot} \text{ yr}^{-1}$, still a typical value for LIRGs.

Although other BLAST counterparts lack shorter wavelength data, we use the results from IRAS 03152–4427 as an upper value on their possible luminosity and temperature to help the fitting procedure. We find that the typical cluster members detected at BLAST wavelengths have temperatures of the order of 15 K, far-IR luminosities of the order of $10^{10} L_{\odot}$ and dust masses around $10^8 M_{\odot}$. Their SFR amounts to a few ($\lesssim 3$) solar masses per year (a few more if the values derived from the UV are also taken into account). Table 3 shows the results of the fit for each of the selected cluster member, including the derived SFR, dust and stellar mass, and SSFR. Our results show that typical BLAST sources in A3112 are mostly normal star-forming galaxies with low SFRs. Fainter submm

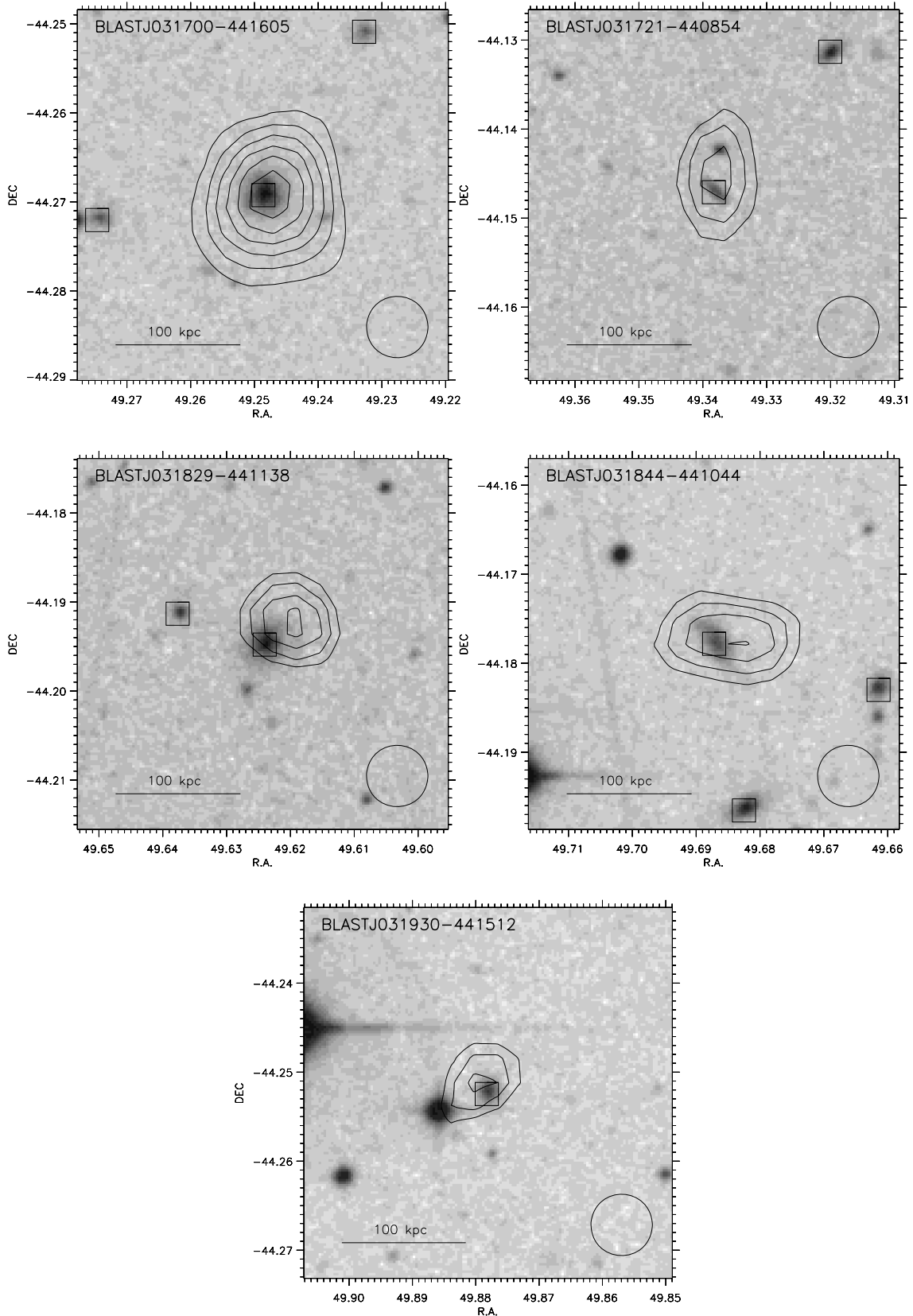
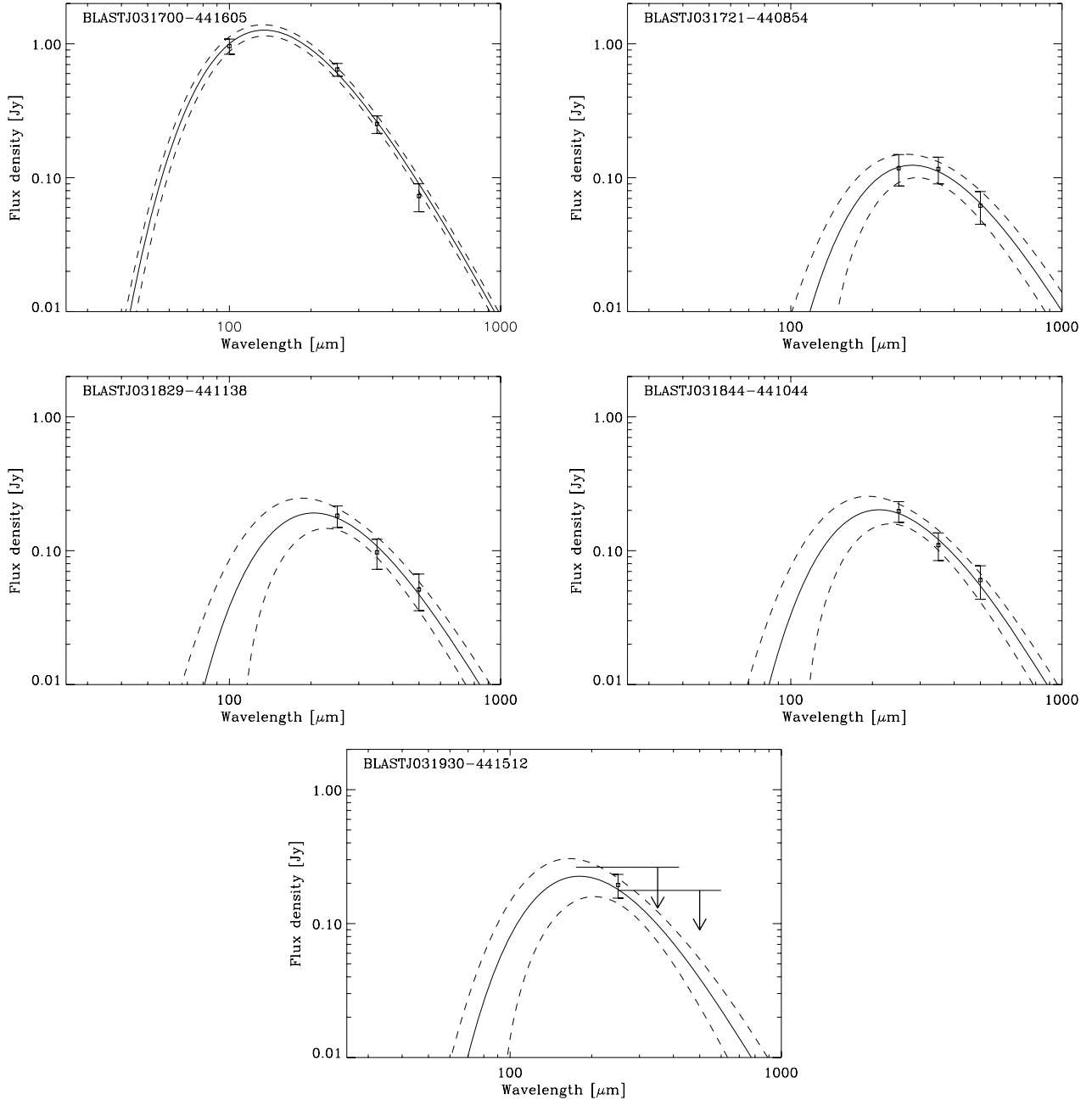


Figure 6. The five cluster members identified as counterparts to 250- μm sources. The background images are cutouts from the DSS-digitized plates. Boxes mark the position of cluster members and contours show 250- μm emission above a threshold of 3σ (82 mJy at 250 μm). The circle in the lower right-hand corner shows the BLAST 250- μm beam size (36 arcsec FWHM). The distance scale is calculated at the cluster redshift. The galaxy in the upper left-hand panel is also an *IRAS* source (*IRAS* 03152-4427).

Table 2. Flux densities (in mJy) at 250, 350 and 500 μm for the cluster members identified as counterparts to 250- μm sources. An asterisk (*) denotes a 3σ upper limit.

Source	S_{100}	δS_{100}	S_{250}	δS_{250}	S_{350}	δS_{350}	S_{500}	δS_{500}
BLAST J031700–441605	960	125	665	29	245	22	79	16
BLAST J031721–440854	–	–	114	28	113	22	64	15
BLAST J031829–441138	–	–	181	28	94	21	54	15
BLAST J031844–441044	–	–	195	28	106	21	63	16
BLAST J031930–441512	–	–	195	34	64*	–	46*	–

**Figure 7.** The submm and far-IR SEDs of the five cluster members identified as counterparts to 250- μm sources. The solid line shows the best fit to the SED and the dashed lines mark the 1σ error intervals obtained using a Monte Carlo sampling of the parameter space.

sources in the cluster are expected to show even lower star formation activity than the galaxies which are individually detected.

Comparison with previous results (e.g. the *ISO* observations of Virgo by Popescu et al. 2002) shows that the dust masses are consis-

tent with other observations; our galaxies have dust masses typical of large early-type spirals. This is in agreement with the bright magnitude of these systems, with their optical colours (cf. Section 3.3) and with their disc-like optical appearance (Fig. 6).

Table 3. Result of the fit to the SEDs of the cluster members identified as counterparts to 250- μm sources. The first object is IRAS 03152–4427, whose fit also includes an *IRAS* data point at 100 μm . Fits for the remaining objects use only BLAST data points. Units are as follows: T is in K; L_{FIR} is in $10^{10} L_{\odot}$; SFR is in $M_{\odot} \text{yr}^{-1}$; and M_{d} is in $10^8 M_{\odot}$. The estimated values of stellar mass M_{s} in units of $10^9 M_{\odot}$ and SSFR in units of Gyr^{-1} are also tabulated.

Source	T	L_{FIR}	SFR_{FIR}	$\text{SFR}_{\text{FIR+UV}}$	M_{d}	M_{s}	SSFR
BLAST J031700–441605	23.4	12.0	20.2	39.7	1.7	14.4	2.76
BLAST J031721–440854	11.2	1.0	1.0	2.0	7.7	3.8	0.53
BLAST J031829–441138	15.8	1.7	2.5	8.8	2.1	6.6	1.33
BLAST J031844–441044	15.1	1.6	2.3	7.0	2.7	5.0	1.40
BLAST J031930–441512	17.3	1.6	2.4	9.1	1.7	7.6	1.20

To evaluate possible contamination from active galactic nuclei (AGNs) in these sources, we use the classification scheme outlined by Kewley et al. (2006) on the Baldwin–Phillips–Terlevich (BPT, Baldwin, Phillips & Terlevich 1981) diagrams, based on the emission-line ratios $[\text{O III}]/\text{H}\beta$, $[\text{N II}]/\text{H}\alpha$, $[\text{S II}]/\text{H}\alpha$ and $[\text{O I}]/\text{H}\alpha$. Using as a reference the curves defined by Kewley et al. (2001) and Kauffmann et al. (2003) (cf. Fig. 8), we see that three of the five BLAST counterparts (BLAST J031700–441605, BLAST J031829–441138 and BLAST J031844–441044) are identified in the $([\text{O III}]/\text{H}\beta)$ versus $([\text{N II}]/\text{H}\alpha)$ plane as combined sources, that is, star-forming galaxies with a possible AGN component. However, all five are classified as normal H II-dominated galaxies according to the $([\text{O III}]/\text{H}\beta)$ versus $([\text{S II}]/\text{H}\alpha)$ criterion, while in the $([\text{O III}]/\text{H}\beta)$ versus $([\text{O I}]/\text{H}\alpha)$ plane, only BLAST J031844–441044 lies in the region occupied by Seyferts and low-ionization nuclear emission-line region galaxies. This confirms that the BLAST counterparts are normal star-forming galaxies; even BLAST J031844–441044, the only source with a mixed profile of star formation and nuclear activity, is clearly identified as hosting an AGN only in one of the three diagrams, thus suggesting that the main source for its submm emission is still star formation. Fig. 9 shows the rest-frame AAOmega spectra of the BLAST counterparts with significant emission lines marked.

3.2.2 Far-IR emission from the brightest cluster galaxy

The brightest cluster galaxy (BCG) in A3112 exhibits strong optical line emission and a powerful, core-dominated radio source. It was targeted with *Spitzer* IRAC and MIPS observations by Quillen et al. (2008) who find a weak mid-IR excess at 24 μm . They derived an infrared luminosity of $2.2 \times 10^{10} L_{\odot}$, which equates to an SFR of $4 M_{\odot} \text{yr}^{-1}$ (O’Dea et al. 2008).

The same diagnostics used for the BLAST counterparts mark the BCG as an AGN-dominated source (Fig. 8). Its optical spectrum is fairly typical of central cluster galaxies, being dominated by emission lines of low-ionization species ($[\text{O I}]$, $[\text{O III}]$ and $[\text{S II}]$), with a relatively low $\text{H}\alpha$ intensity (Fig. 10).

The BLAST results are at face value inconsistent with the SFR from *Spitzer*, with a 2σ detection at 250 μm of $57 \pm 28 \text{ mJy}$, and upper limits of 64 and 46 mJy at 350 and 500 μm (assuming three times the map rms), respectively. This translates to an upper limit of $3.1 \times 10^9 L_{\odot}$ for the far-IR luminosity and $0.6 M_{\odot} \text{yr}^{-1}$ for the SFR. However, the *Spitzer* and BLAST luminosities are derived using different methods, and the *Spitzer*-derived value is potentially overestimated due to the mid-IR contribution of an AGN. The presence of an AGN is consistent with the results of Takizawa et al. (2003) who find an X-ray point source, with a power-law index 1.9, coincident with

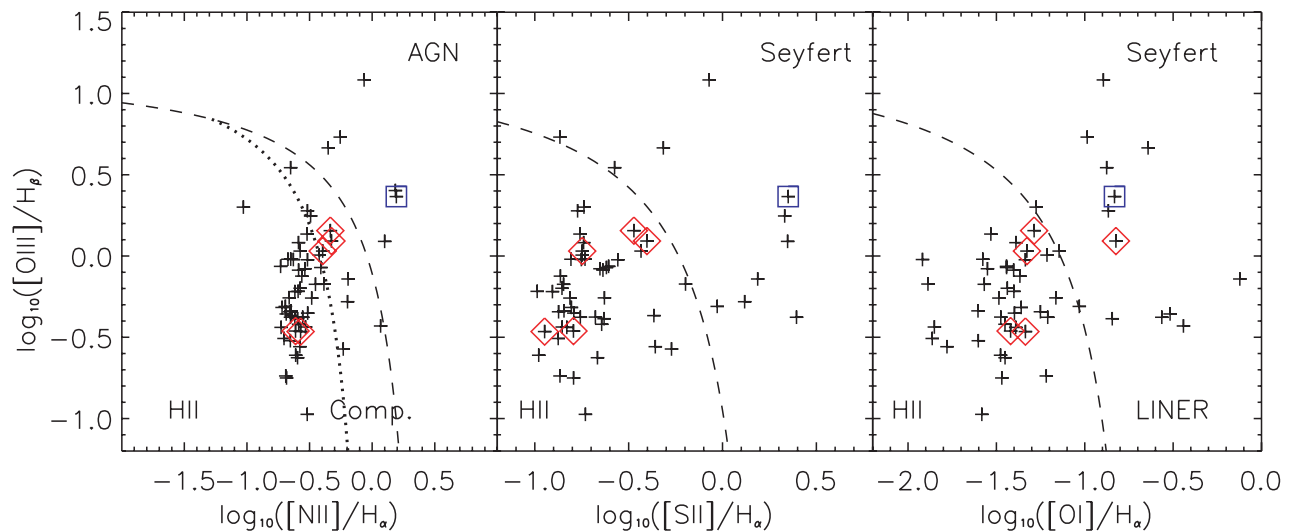


Figure 8. The spectroscopic members of A3112 in the BPT diagnostic diagrams. Diamonds mark the position of the five BLAST counterparts; the box marks the cluster BCG (see Section 3.2.2). The dashed lines mark the starburst–AGN separation tracks of Kewley et al. (2001), while the classification separator of Kauffmann et al. (2003) is shown as a dotted line in the left-hand panel.

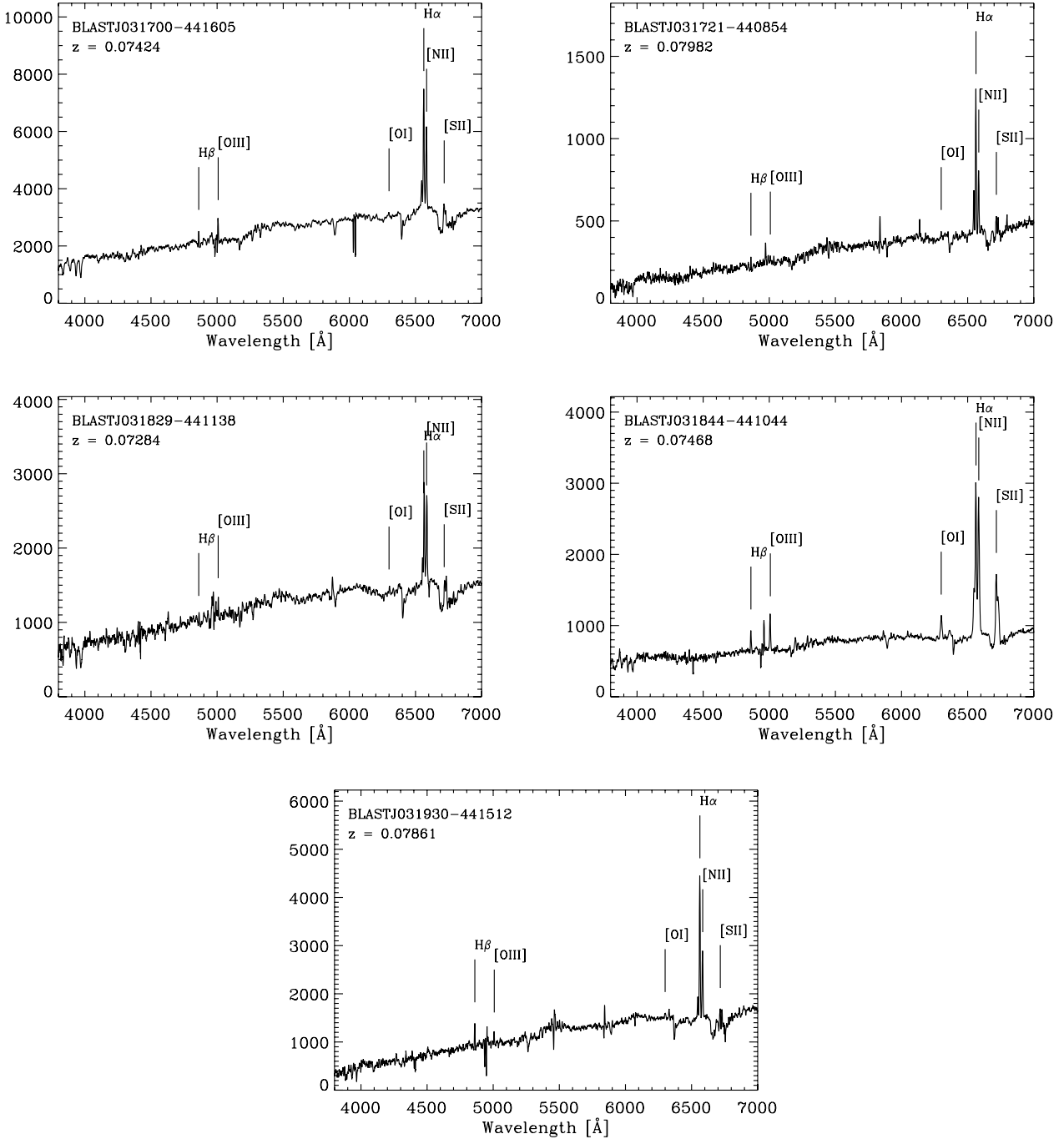


Figure 9. Optical spectra of the five cluster members identified as counterparts to 250- μm sources. Vertical lines mark interesting spectral lines used for diagnostics: $\text{H}\beta$ ($\lambda = 4861 \text{ \AA}$), $[\text{O III}]$ ($\lambda = 5008 \text{ \AA}$), $[\text{O I}]$ ($\lambda = 6300 \text{ \AA}$), $\text{H}\alpha$ ($\lambda = 6563 \text{ \AA}$), $[\text{N II}]$ ($\lambda = 6584 \text{ \AA}$) and $[\text{S II}]$ ($\lambda = 6717 \text{ \AA}$). The spectra have been smoothed with a boxcar of 5 pixels; units are instrumental counts.

the core of the BCG. The BLAST limit is at the lower end of the SFR values found both by O’Dea et al. (2008) and by us with the UV detection of the BCG by the *GALEX* ($1.5 M_{\odot} \text{ yr}^{-1}$, cf. Section 3.1), so the mid-IR-to-far-IR flux ratio is not consistent with star formation alone.

Therefore, the mid-IR flux from BCG in A3112 is predominantly from the AGN as found in a small fraction (four out of 62) of the O’Dea et al. (2008) sample, but unlike those the AGN is a strong radio source.

3.3 BLAST sources along the colour–magnitude diagram

The cluster colour–magnitude diagram (CMD) enables us to select galaxies with respect to their overall unobscured star formation activity. As already pointed out in Section 3.1, a large number of objects lie on the cluster RS, identifying them as passively evolving ellipticals. Moreover, we find the region redwards of the RS to be populated by 26 galaxies (i.e. 18 per cent of the optical sample) showing colours about 0.1–0.2 mag redder than the RS. The

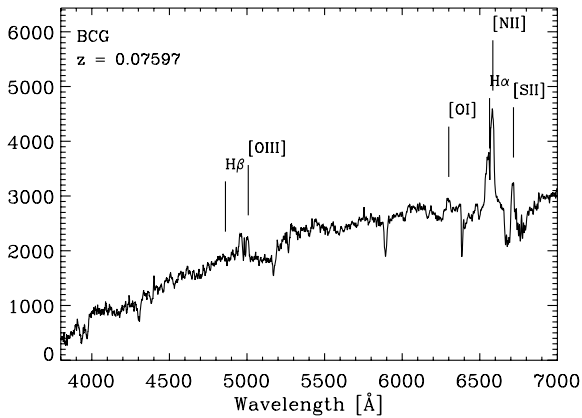


Figure 10. Optical spectrum of the BCG in A3112. Vertical lines mark spectral lines used for diagnostics (see Fig. 9). The spectrum has been smoothed with a boxcar of 5 pixels; units are instrumental counts.

combination of the BLAST with optical and near-IR data can help in understanding the nature of these systems.

We thus stack the three subcatalogues of blue galaxies (21 objects below the RS), RS galaxies (99 objects) and very red galaxies (26 objects redder than the RS). We then derive the mean SFR from the far-IR luminosity, as in Section 3.2. The results are presented in Table 4, showing that the majority of the stacked submm emission from our cluster member catalogue comes from optically blue (i.e. star-forming) galaxies. The bulk of their emission is clearly detected at $250\ \mu\text{m}$. On the other hand, RS galaxies show no significant emission in any BLAST band, confirming these systems as largely evolved, dust-free galaxies; consistently, their derived SFR is negligible. The very red galaxies also show little submm emission, mostly consistent with zero, although with large error bars. The inferred SFR is therefore also very low. This suggests that this population is overall depleted of cold dust.

Additional information about the very red galaxies can be inferred from the comparison of their optical and near-IR properties. We find that the $(J - K_S)$ colour of these galaxies is largely consistent with the colour of the RS in the $(J - K_S)$ versus K_S plane, confirming these galaxies to have an old stellar population typical of RS galaxies. Moreover, most of them are found in the central regions of the cluster, where very few young dusty galaxies are expected on average for a non-merging, relaxed cluster like A3112. This suggests that the observed red optical colour could arise from other factors than isotropic dust reddening.

Several authors in the recent past have shown, using both radiative transfer models (Pierini & Möller 2003; Pierini et al. 2004) and observational data (e.g. Driver et al. 2007), that more or less severe reddening can arise depending on galaxy geometry and orientation. Both Pierini et al. (2004) and Driver et al. (2007) show that attenuation is largely dependent on the observed wavebands, with stronger effects in the bluer bands. A strong contribution is also due to galaxy morphology, the bulge-to-disc ratio playing an important role in determining the overall effect on the observed colours. For intermediate inclination angles ($i < 60^\circ$), the ratio of the colour terms $E(B - V)/E(J - K)$ is higher for discs than for bulges. Discs also show overall lower colour terms, regardless of the structure of interstellar dust.

The geometrical parameters derived from SExtractor (namely the semimajor axis, a , and semiminor axis, b , of the largest ellipsoidal isophote encircling the galaxy) can be used to roughly estimate the inclination angle of the galaxy along the line of sight

Table 4. Results of stacking for the three colour-selected catalogues. Fluxes are in mJy; SFR is in $M_\odot\ \text{yr}^{-1}$.

Catalogue	S_{250}	δS_{250}	S_{350}	δS_{350}	S_{500}	δS_{500}	SFR
Blue	29	6	9	5	4	3	1.7
RS	6	3	4	2	2	1	0.2
Red	4	5	0	4	6	3	0.1
RS + Red	5	3	3	2	2	1	0.2

(if the observed galaxy is approximated as a disc of radius $R = a$, the inclination angle along the line of sight can be expressed as $\theta_{\text{los}} = [(90^\circ/2\pi)a \cos(b/a)]$). We find that the very red galaxies all have inclination angles between 30° and 60° . This suggests that these galaxies could appear reddened by superposition of a thick disc over a relatively small bulge. In this case, the expected attenuation coefficient is almost negligible in the near-IR, while it can range from 0.2 to about 0.5 in the B band. We thus interpret the very red galaxies as discs with an overall evolved stellar population (i.e. belonging to the RS) and relatively low dust content, which are preferentially reddened because of their inclination. Following this, we stack the submm maps on the combined catalogue of red and RS galaxies, considering them as a single population. We see that the addition of very red galaxies results in a mean SED consistent with that from RS galaxies. Results of stacking are reported in Table 3.

To better characterize the nature of the optical counterparts to the bright BLAST sources, we investigate their location in the CMD and their optical colours. Fig. 4 shows the position in the CMD of the cluster members identified as BLAST counterparts. These five galaxies all lie in a narrow region of the CMD, with a mean colour $(B - R) = 1.38 \pm 0.08$ and K_S magnitudes below K_S^* (excluding IRAS 03152–4427, which has a magnitude of the order of K_S^*).

3.4 Radial distribution of submm emission

Several studies have revealed the presence of trends in the star formation activity of cluster galaxies with respect to the clustercentric radius. This is usually interpreted as a combination of environmental effects that trigger star formation episodes in galaxies infalling on the cluster from the field. Investigating the radial distribution of submm emission from cluster members can help in better understanding how the environment affects cluster galaxies and to what extent these effects are detected at far-IR wavelengths.

We thus divide our spectroscopic catalogue of 146 cluster members into radial bins centred on the BCG, whose position is coincident with the dynamical centre of the cluster. We define the bins so that each contains similar numbers of objects to ensure homogeneous stacking statistics. We find that 25 galaxies per bin is a good compromise between the number of bins (6) and S/N.

The radial plot of the mean stacked flux density (see Fig. 11) shows two significant ($\sim 4\sigma$) peaks at $250\ \mu\text{m}$. The outermost of these peaks is detected at about $1.5R_{200}$, that is, outside the gravitational radius of the cluster (this region is only covered by the shallower part of the BLAST map and thus the stacking results are quite noisy). This is expected, since at radii $\gtrsim R_{200}$ the infall of galaxies from the field is expected to be most notable and thus an increase in the mean SFR is expected (e.g. Balogh et al. 1999). This signal drops at longer wavelengths.

A second peak is detected closer to the cluster core, around $0.6R_{200}$. To investigate whether this peak is genuinely due to the presence of the cluster, we use the same method and stack the BLAST-BGS map (Devlin et al. 2009) on simulated catalogues.

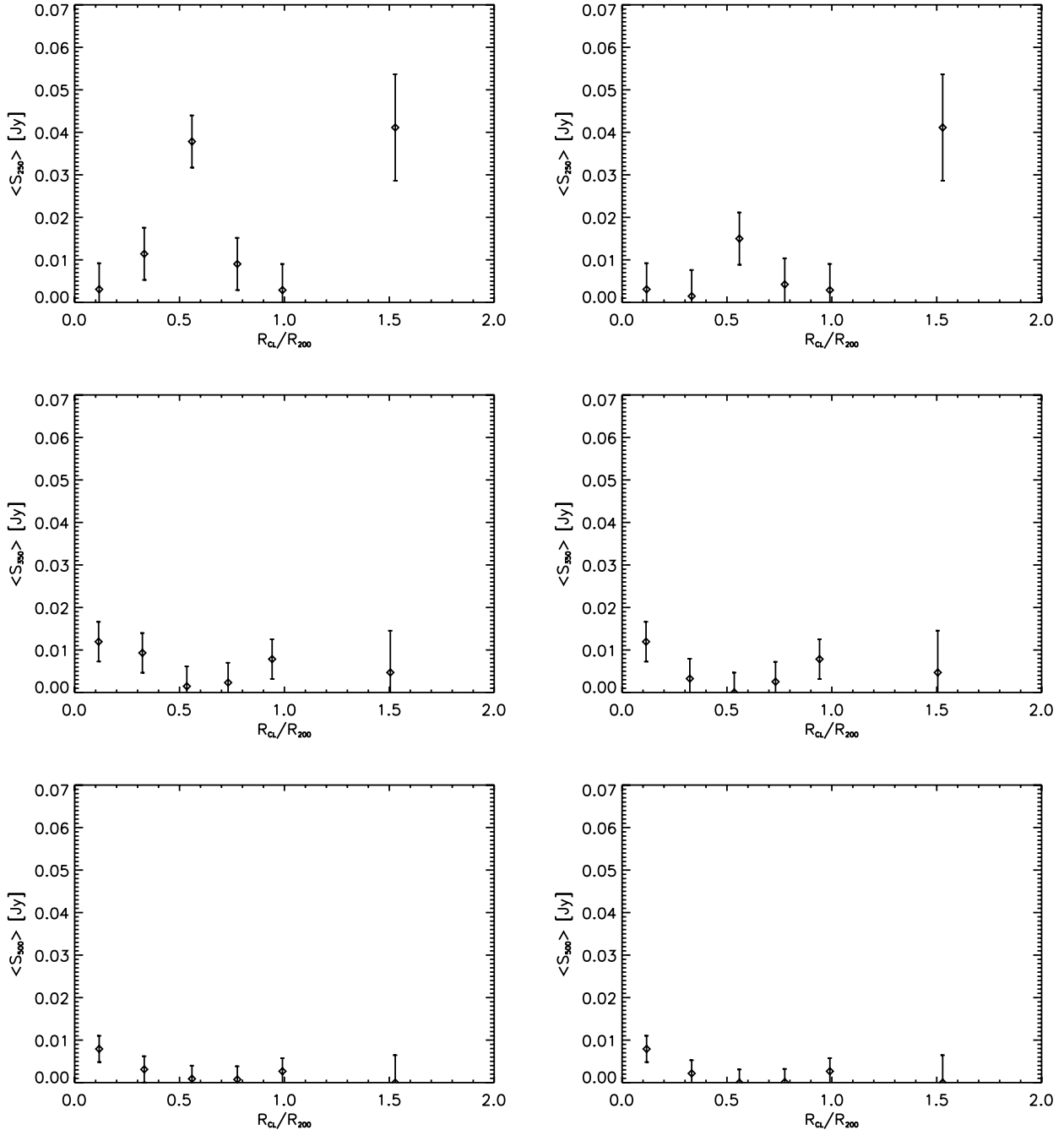


Figure 11. Stacked BLAST flux density of cluster members in bins of different clustercentric radii (1σ error bars). The left-hand panels show the result of stacking the BLAST maps on all cluster members. The right-hand panels show the stacking after removal of cluster members individually detected at submm wavelengths. Top row: stacking of the 250- μm map. Middle row: stacking of 350- μm map. Bottom row: stacking of the 500- μm map. A significant increase in the mean submm flux density is detected around $0.6R_{200}$ at 250 μm , along with another increase beyond R_{200} .

Since the BGS is a blank field, we can use it to assess the probability of random occurrence of a radial peak with the same significance as detected in A3112. We thus generate 10 000 sets of 146 positions, randomly distributed around a centre and on an area equivalent to the map of A3112, stack the BGS map on each, look for the presence of a radial peak and calculate its deviation from the mean of the radial profile. To test if the presence of a cluster affects the outcome of the stacking analysis, we also simulate 10 000 catalogues of 146 normally distributed positions over the same area (we use the value of R_{500} found for A3112 as the standard deviation of the distribution

to roughly reproduce a density profile consistent with the presence of a cluster). We find that the probability of random occurrence of a peak as significant as that detected in A3112 is less than 10^{-5} in all cases. Limiting this analysis to the BGS-Deep or BGS-Wide maps also yields similar results.

To check independently the significance of this peak, we also compare the stacked values with two radial profiles: a flat profile with value equal to the mean of the stacked values and a Gaussian-shaped profile, which we assume as a representation of the peak. A Kolmogorov–Smirnov test shows that the flat profile is ruled out

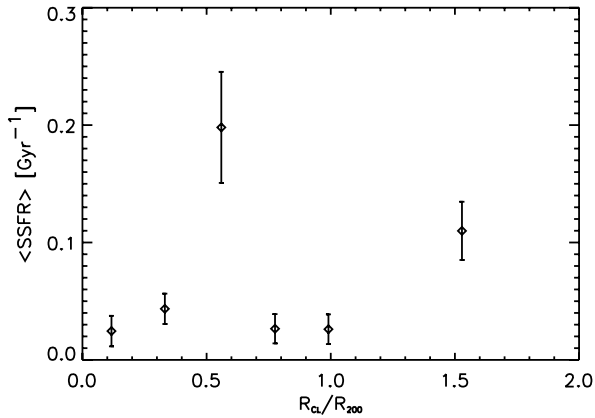


Figure 12. Radial profile of the averaged SSFR of cluster members. A significant increase is detected around $0.6R_{200}$.

with a rejection probability of 0.9996, while a peaked profile is accepted with very high probability (rejection of 9×10^{-4}). We also test the same profiles by stacking in smaller radial bins (12–20 objects per bin); although the data are noisier due to lower statistics, the flat profile is still ruled out, while the peaked profile provides a good fit.

We also note that the cluster members matching the position of 250- μm -detected sources mostly lie at the distance of the inner radial peak. These galaxies do not appear to be clustered among themselves, being instead randomly distributed azimuthally. In order to evaluate whether the peak is entirely due to the presence of these galaxies, we stack our catalogue after removing them. Although the peak shows a lower deviation from the mean value ($\sim 2\sigma$), a flat profile again has a low probability of being a good representation of the data (although with a lower rejection probability of 0.3). A peaked profile has again a very low rejection probability (1.3×10^{-3}), thus providing a robust representation of the data.

The same analysis on the 350- and 500- μm data shows no significant peak at the same position, although a minimum is notable at both wavelengths. We assess the statistical significance of these minima as negligible ($\lesssim 2\sigma$ at 350 μm , $\lesssim 1\sigma$ at 500 μm), which points to low statistics as the main origin for this behaviour. Also, the SEDs of BLAST-detected cluster members do not show any notable drop at longer wavelengths, thus ruling out the galaxies themselves as the origin of the minimum.

In addition to that, cluster members from the innermost bin show on average a non-zero mean flux density. The fact that this is mostly seen at 350 and 500 μm suggests a mild degree of superposition with background sources, again notable because of small number statistics. The significance of this signal is nevertheless low ($\sim 1.5\sigma$).

To ensure that no selection effect in the input catalogue is biasing this result, we also investigate the $(B - R)$ colour of galaxies in each bin. We find that all radial bins (but the innermost) are populated by a mix of red-sequence and blue galaxies, thus assuring that the peak is not due to undersampling of blue (i.e. star-forming) galaxies at radii of the order of R_{200} . The number of blue galaxies is indeed essentially the same (four to five) in all radial bins.

From the stacked flux profiles, we also derive a radial profile of averaged SSFR, where the SSFR is the SFR normalized to the mass of the galaxy (here we use the stellar mass value derived from the K_S magnitudes). The profile (Fig. 12) shows again the same peak, confirming that the detected peak matches an intrinsic increase in the star formation activity of cluster galaxies around $0.6R_{200}$.

3.5 Submm emission across the luminosity function

We can also stack maps on the spectroscopic catalogue of cluster members, after dividing into bins of absolute K_S magnitude, to study how the submm BLAST flux is distributed across the cluster luminosity/mass function. Although the available data do not allow us to probe the dwarf population of cluster members, they cover three full magnitudes in the K_S band, enough to reach intermediate-luminosity galaxies down to $K_S^* + 2$. As in the case of radial stacking, we define magnitude bins containing a constant number of objects (25) for homogeneous stacking statistics.

The result of stacking on magnitude is shown in Fig. 13. A notable peak around magnitudes fainter than K_S^* is immediately evident, with the largest part of the BLAST 250- μm emission originating from galaxies with K_S absolute magnitudes of the order of $K_S^* + 1$. The stacked flux then decreases beyond K_S^* , that is, towards the giant ellipticals. Given the robust correlation between the K_S magnitude and stellar mass, we identify these systems as having stellar masses of the order of a few times $10^9 M_\odot$. Removing the BLAST-detected sources shows that a larger number of galaxies contributes to this signal. Stacking the 350- μm map shows a less-strong signal, although the transition across K_S^* is still notable. Removal of the BLAST counterparts does not change the plot significantly. At 500 μm , the mean flux density is consistent with zero at every magnitude.

Again, we derive the average SSFR in each magnitude bin; the profile (Fig. 14) shows a significant increase in the intrinsic star formation activity of cluster members at magnitudes fainter than K_S^* and the rapid drop at magnitudes brighter than K_S^* .

4 DISCUSSION

The combination of optical and submm photometry with statistical results from stacking analyses provides insight into the star formation activity of galaxies in A3112.

We statistically detect the mean submm emission from cluster members, which we quantify as 16.6 ± 2.5 , 6.1 ± 1.9 and 1.5 ± 1.3 mJy at 250, 350 and 500 μm , respectively. These numbers can provide a reference for future, deeper submm observations of other galaxy clusters. The mean SED and SFR derived from the stacking shows that A3112 has a total SFR density of $12.4 \pm 3.4 M_\odot \text{yr}^{-1} / (10^{14} M_\odot)$. This is in good agreement with previous results on other clusters (Geach et al. 2006; Haines et al. 2009b) and suggests that submm data can help in reducing the scatter in measurements of the evolution of the SFR versus redshift for galaxy clusters.

The results from clustercentric radial stacking show that a large fraction of the total star formation activity in the cluster is taking place at specific clustercentric distances. At radii beyond R_{200} , a large amount of signal is detected, preferentially at 250 μm . Previous optical studies of star formation activity in clusters have shown the presence of radial trends in the relative proportions of star-forming and passive galaxies, across mass scales covering the full range from groups to superclusters (e.g. Balogh et al. 1999; Porter & Raychaudhury 2007; Porter et al. 2008; Wilman et al. 2008; Braglia et al. 2009). It is now well established that at distances of the order of R_{200} , the SFRs of infalling galaxies can experience a more- or less-prolonged period of enhanced activity, mainly due to environmental effects. This is also consistent with the statistical analysis of BLAST sources of Viero et al. (2009) who detect a spatial correlation length of 4.9 ± 0.7 Mpc for 250- μm sources. This loosely corresponds to about $2R_{200}$ for A3112, consistent with the distance

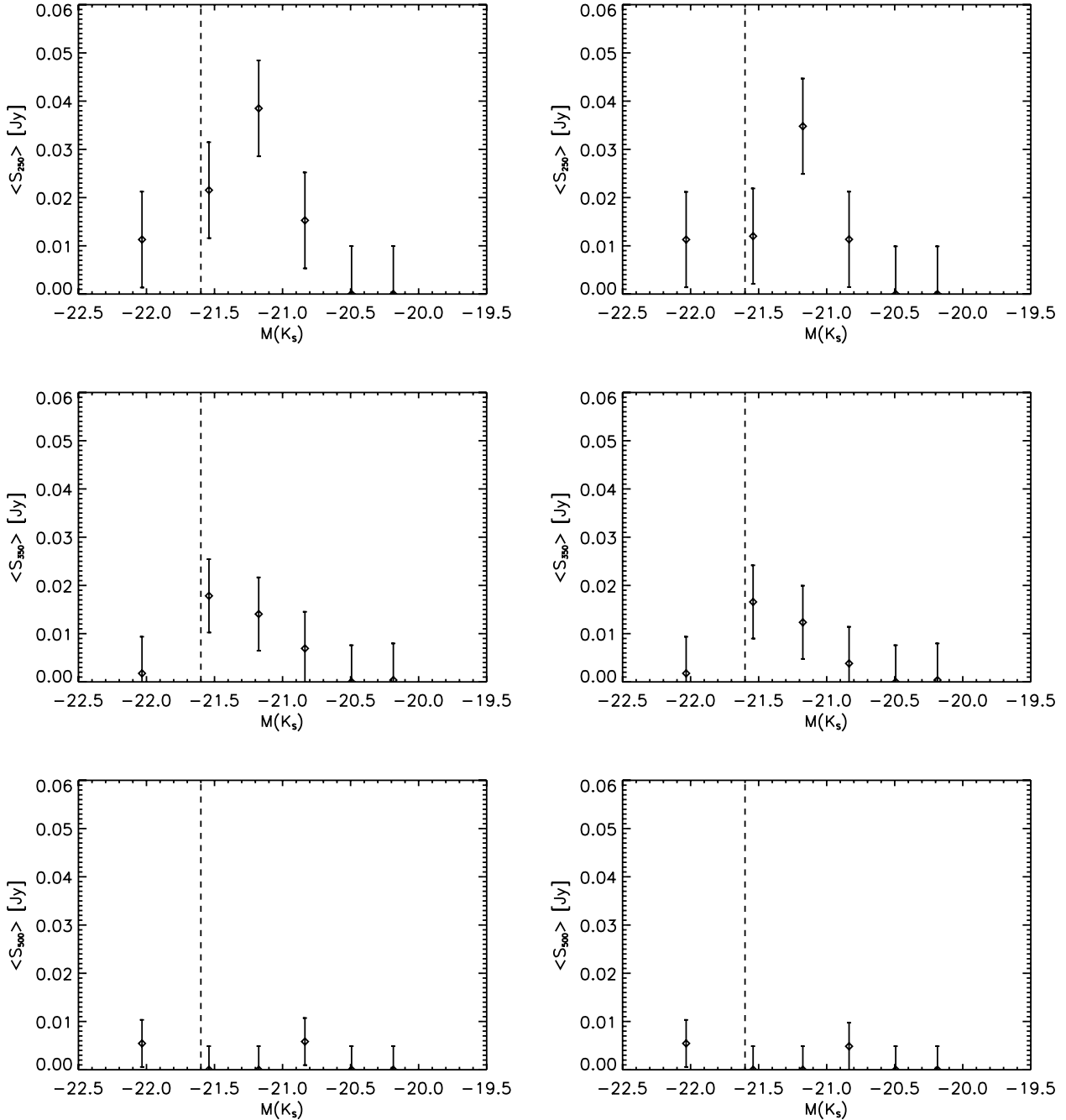


Figure 13. Stacked flux density of cluster members in bins of absolute K_S magnitude. The left-hand panels include all cluster members; the right-hand panels exclude the individual sources. The dashed line marks the position of the characteristic magnitude K_S^* . Top row: stacking of the 250- μm map. Middle row: stacking of the 350- μm map. Bottom row: stacking of the 500- μm map.

of the outermost radial bin in our analysis. The detected signal is thus well explained within the general picture of galaxy infall on to clusters.

In addition, at around $0.6R_{200}$, a significant enhancement in the star formation activity is detected at BLAST wavelengths. This radius roughly corresponds to R_{500} (Sanderson et al. 2003), that is, the boundary between the infall region and the virialized cluster core. The recent investigations of galaxy clusters with *Spitzer* have shown that the radial trends detected at optical wavelengths in fact extend deeper into the cluster core, both in filamentary structures (Fadda et al. 2008) and in the infall regions between R_{200} and R_{500} (Bai et al.

2007; Saintonge et al. 2008; Haines et al. 2009a,b; Tran et al. 2009). In all cases, a global decrease in the fraction of mid-IR luminous galaxies is seen towards the innermost regions of clusters, which is usually interpreted in terms of gradual quenching by environmental effects due to interaction with other cluster members and with the diffuse intracluster gas. Our observations in the submm confirm this picture also, at wavelengths which sample a region close to the far-IR peak of the cold dust, which is heated directly by the UV radiation of O and B stars. Although a large fraction of the submm emission detected is clearly due to the cluster members individually detected at submm wavelengths, we see evidence from stacking of

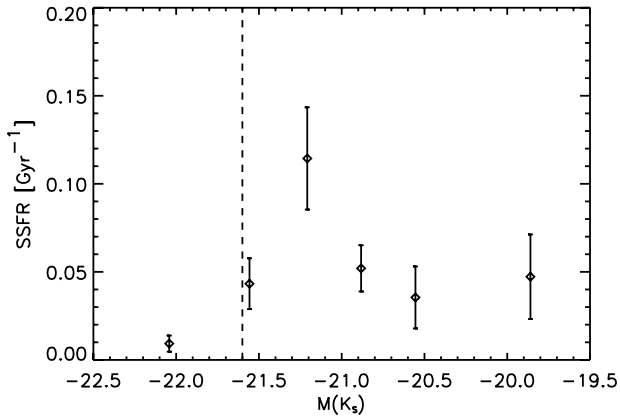


Figure 14. Average SSFR in bins of absolute K_S magnitude. The dashed line marks the position of the cluster's characteristic magnitude K_S^* .

a larger population of galaxies whose submm emission is statistically detected at around R_{500} . This suggests that, on average, cluster galaxies are expected to show an overall enhanced star formation level at this distance, once again mainly due to environmental effects in the densest cluster regions.

The distribution of mean submm emission with respect to galaxy K_S magnitude shows that a significant fraction of star formation is carried by systems with $K_S > K_S^*$, that is, by intermediate-mass galaxies. The mean submm flux density is seen to increase towards more luminous K_S magnitudes, until a notable drop at the brightest magnitudes (as expected for passively evolving ellipticals). This agrees with previous results (e.g. Pierini & Möller 2003) and shows that a large part of the star formation activity is taking place in intermediate systems. The depth of our spectroscopic catalogue does not allow us to probe the dwarf regime; thus, we cannot rule out the presence of additional star formation taking place in lower mass systems.

Analysis of individual sources, as well as stacking against colour criteria, allows us to assess the nature of the cluster members detected by the BLAST. Excluding the single galaxy IRAS 03152–4427, which is identified as a LIRG with a relatively high temperature of 23.4 K and a total SFR of $39 M_{\odot} \text{ yr}^{-1}$, both the SEDs of individual sources and the stacked SED show that typical star-forming galaxies in A3112 are not undergoing strong star formation activity, but instead are identified as normal star-forming galaxies with total SFRs of a few (< 10) $M_{\odot} \text{ yr}^{-1}$, far-IR luminosities of the order of $10^{10} L_{\odot}$ and temperatures below 20 K. Their total dust mass is of the order of $10^8 M_{\odot}$, typical of large spirals. Optical classification of these galaxies reveals them to be massive [$M_{\text{Star}} \sim (5-10) \times 10^9 M_{\odot}$], disc-like galaxies with relatively red colours. Recent studies have shown the presence of dusty red spirals with mild star formation in the overdense regions of clusters (e.g. Gallazzi et al. 2009): the SSFR of the BLAST counterparts, of the order of Gyr^{-1} , is consistent with this classification. Spectroscopic analysis based on emission-line ratios independently confirms these objects to be normal star-forming galaxies, with only BLAST J031844–441044 showing a mild AGN contribution. The CMD reveals that they all lie in a narrow colour strip with $(B - R) = 1.38 \pm 0.08$, that is, at an interface region between the population of star-forming galaxies and the old passively evolving galaxies on the RS. The population of galaxies with $(B - R)$ colour redder than the RS is revealed to be composed of quiescent galaxies, whose redder colour is probably due to geometrical properties rather than increased levels of dust.

5 CONCLUSIONS AND SUMMARY

We have been able to provide a description of the star formation activity of member galaxies in a cluster at submm wavelengths, as observed by the BLAST experiment. A combination of stacking analyses based on the clustercentric distance, galaxy magnitude and colour allowed us to identify correlations between optical properties of cluster galaxies and their FIR emission.

Studying the submm SEDs and optical spectra of cluster members identifies BLAST-detected cluster members mostly as normal star-forming galaxies. Their optical colour, spectroscopic properties and K_S magnitude identify them as massive early-type galaxies in an advanced stage of evolution. The BCG is found to have low dust content, its mid-IR emission being dominated by the central AGN.

Together with an expected increase in the SFR in the cluster outskirts, we find a significant increase in the $250 \mu\text{m}$ flux density at distances around R_{500} , that is, further inside the cluster with respect to the infall region. The increase peaks to values three to four times as large as in the inner regions of the cluster. This confirms previous studies in the mid-IR that show large fractions of star-forming galaxies closer to the dense cores of galaxy clusters. The combined results of our analysis show that the cluster members identified at submm wavelengths can be part of a population of evolved systems on the verge of transition from the population of blue active galaxies to the quenched systems (ellipticals and S0s) dominating the cluster cores and suggest that environmental effects at distances of the order of R_{500} play a role regulating star formation activity during this transition.

Deeper and more complete studies of galaxy clusters at far-IR and submm wavelengths with *Herschel* and the SCUBA-2 will provide more complete coverage of physical processes at work in cluster galaxies. In particular, combining the higher sensitivity and resolution of the SPIRE, and the spectral coverage offered by parallel observations with the PACS and SPIRE will allow the detection and characterization of cluster galaxies down to lower luminosities and masses, providing a more complete description of the star formation activity in galaxy clusters.

ACKNOWLEDGMENTS

We acknowledge the support of the National Aeronautics and Space Administration (NASA) through grant numbers NAG5-12785, NAG5-13301 and NNGO-6G111G, the NSF Office of Polar Programs, the Canadian Space Agency, the Natural Sciences and Engineering Research Council (NSERC) of Canada, and the UK Science and Technology Facilities Council (STFC). This research has been enabled by the use of WestGrid computing resources. FGB acknowledges Daniele Pierini for helpful discussions and the anonymous referee for their suggestions. This work is partly based on observations made at the Australian Astronomical Observatory with the Anglo-Australian Telescope. This research has made use of the NED, which is operated by the Jet Propulsion Laboratory, California Institute of Technology, under contract with the NASA. This publication makes use of data products from the 2MASS, which is a joint project of the University of Massachusetts and the Infrared Processing and Analysis Center/California Institute of Technology, funded by the NASA and the National Science Foundation. This work is based in part on observations made with the *Spitzer Space Telescope*, which is operated by the Jet Propulsion Laboratory, California Institute of Technology under a contract with the NASA.

REFERENCES

- Arnouts S. et al., 2007, *A&A*, 476, 137
 Bai L., Rieke G. H., Rieke M. J., 2007, *ApJ*, 668, L5
 Baldwin J. A., Phillips M. M., Terlevich R., 1981, *PASP*, 93, 5
 Balogh M. L., Morris S. L., Yee H. K. C., Carlberg R. G., Ellingson E., 1999, *ApJ*, 527, 54
 Bell E. F., 2003, *ApJ*, 586, 794
 Biviano A., Murante G., Borgani S., Diaferio A., Dolag K., Girardi M., 2006, *A&A*, 456, 23
 Böhringer H. et al., 2004, *A&A*, 425, 367
 Braglia F., Pierini D., Böhringer H., 2007, *A&A*, 470, 425
 Braglia F. G., Pierini D., Biviano A., Böhringer H., 2009, *A&A*, 500, 947
 Chapin E. L. et al., 2008, *ApJ*, 681, 428
 Cole S. et al., 2001, *MNRAS*, 326, 255
 Colless M. et al., 2001, *MNRAS*, 328, 1039
 Cowie L. L., Barger A. J., Fomalont E. B., Capak P., 2004, *ApJ*, 603, L69
 den Hartog R., Katgert P., 1996, *MNRAS*, 279, 349
 Devlin M. J. et al., 2009, *Nat*, 458, 737
 Dressler A., 1980, *ApJ*, 236, 351
 Dressler A. et al., 1997, *ApJ*, 490, 577
 Driver S. P., Popescu C. C., Tuffs R. J., Liske J., Graham A. W., Allen P. D., de Propriis R., 2007, *MNRAS*, 379, 1022
 Dunlop J. S. et al., 2010, *MNRAS*, 408, 2022
 Dye S. et al., 2009, *ApJ*, 703, 285
 Edge A. C., 2001, *MNRAS*, 328, 762
 Fadda D., Biviano A., Marleau F. R., Storrie-Lombardi L. J., Durret F., 2008, *ApJ*, 672, L9
 Gallazzi A. et al., 2009, *ApJ*, 690, 1883
 Geach, et al., 2006, *ApJ*, 649, 661
 Giard M., Montier L., Pointecouteau E., Simmat E., 2008, *A&A*, 490, 547
 Girardi M., Biviano A., Giuricin G., Mardirossian F., Mezzetti M., 1993, *ApJ*, 404, 38
 Haines C. P. et al., 2009, *ApJ*, 704, 126
 Haines C. P., Smith G. P., Egami E., Okabe N., Takada M., Ellis R. S., Moran S. M., Umetsu K., 2009, *MNRAS*, 396, 1297
 Ivison R. J. et al., 2007, *MNRAS*, 380, 199
 Ivison R. J. et al., 2010, *MNRAS*, 402, 245
 Katgert P., Biviano A., Mazure A., 2004, *ApJ*, 600, 657
 Kauffmann G. et al., 2003, *MNRAS*, 346, 1055
 Kewley L. J., Dopita M. A., Sutherland R. S., Heisler C. A., Trevena J., 2001, *ApJ*, 556, 121
 Kewley L. J., Groves B., Kauffmann G., Heckman T., 2006, *MNRAS*, 372, 961
 Kodama T., Smail I., Nakata F., Okamura S., Bower R. G., 2001, *ApJ*, 562, L9
 Marsden G. et al., 2009, *ApJ*, 707, 1729
 Metcalfe L., Fadda D., Biviano A., 2005, *Space Sci. Rev.*, 119, 425
 Montier L. A., Giard M., 2005, *A&A*, 439, 35
 Moshir M. et al., 1990, *BAAS*, 22, 1325
 O'Dea, et al., 2008, *ApJ*, 681, 1035
 Pascale E. et al., 2008, *ApJ*, 681, 400
 Pascale E. et al., 2009, *ApJ*, 707, 1740
 Patanchon G. et al., 2008, *ApJ*, 681, 708
 Patanchon G. et al., 2009, *ApJ*, 707, 1750
 Pierini D., Möller C. S., 2003, *MNRAS*, 346, 818
 Pierini D., Gordon K. D., Witt A. N., Madsen G. J., 2004, *ApJ*, 617, 1022
 Pimblet K. A., Smail I., Edge A. C., Couch W. J., O'Hely E., Zabludoff A. I., 2001, *MNRAS*, 327, 588
 Pimblet K. A., Smail I., Kodama T., Couch W. J., Edge A. C., Zabludoff A. I., O'Hely E., 2002, *MNRAS*, 331, 333
 Poggianti B. M. et al., 2006, *ApJ*, 642, 188
 Poggianti B. M. et al., 2009, *ApJ*, 693, 112
 Popescu C. C., Tuffs R. J., Völk H. J., Pierini D., Madore B. F., 2002, *ApJ*, 567, 221
 Porter S. C., Raychaudhury S., 2007, *MNRAS*, 375, 1409
 Porter S. C., Raychaudhury S., Pimblet K. A., Drinkwater M. J., 2008, *MNRAS*, 388, 1152
 Quillen A. C. et al., 2008, *ApJS*, 176, 39
 Rex M. et al., 2009, *ApJ*, 703, 348
 Saintonge A., Tran, K.-V. H., Holden B. P., 2008, *ApJ*, 685, L113
 Sanderson A. J. R., Ponman T. J., Finoguenov A., Lloyd-Davies E. J., Markevitch M., 2003, *MNRAS*, 340, 989
 Schiminovich D. et al., 2005, *ApJ*, 619, L47
 Sharp R. et al., 2006, in McLean I. S., Iye M., eds, *SPIE Conf. Ser. Vol. 6269, Ground-based and Airborne Instrumentation for Astronomy. SPIE, Bellingham*, p. 14S
 Shectman S. A., Landy S. D., Oemler A., Tucker D. L., Lin H., Kirshner R. P., Schechter P. L., 1996, *ApJ*, 470, 172
 Skrutskie M. F. et al., 2006, *AJ*, 131, 1163
 Stickel M., Lemke D., Mattila K., Haikala L. K., Haas M., 1998, *A&A*, 329, 55
 Stickel M., Klaas U., Lemke D., Mattila K., 2002, *A&A*, 383, 367
 Takizawa M., Sarazin C. L., Blanton E. L., Taylor G. B., 2003, *ApJ*, 595, 142
 Tran, K.-V. H., Saintonge A., Moustakas J., Bai L., Gonzalez A. H., Holden B. P., Zaritsky D., Kautsch S. J., 2009, *ApJ*, 705, 809
 Truch M. D. P. et al., 2009, *ApJ*, 707, 1723
 Tucker W. et al., 1998, *ApJ*, 496, L5
 Tuffs R. J. et al., 2002, *ApJS*, 139, 37
 Verdugo M., Ziegler B. L., Gerken B., 2008, *A&A*, 486, 9
 Viero M. P. et al., 2009, *ApJ*, 707, 1766
 Wardlow J. L. et al., 2010, *MNRAS*, 401, 2299
 Wiebe D. V. et al., 2009, *ApJ*, 707, 1809
 Wilman D. J. et al., 2008, *ApJ*, 680, 1009

SUPPORTING INFORMATION

Additional Supporting Information may be found in the online version of this article:

Table 1. Combined BLAST catalogue of objects in the field of A3112.

Please note: Wiley-Blackwell are not responsible for the content or functionality of any supporting materials supplied by the authors. Any queries (other than missing material) should be directed to the corresponding author for the article.

This paper has been typeset from a $\text{\TeX}/\text{\LaTeX}$ file prepared by the author.